MIT Open Access Articles

Dynamical Attribution of Recent Variability in Atlantic Overturning

Massachusetts Institute of Technology

Dynamical Attribution of Recent Variability in Atlantic Overturning

Helen R. Pillar[+]

Department of Earth Sciences, University of Oxford, Oxford, United Kingdom

Patrick Heimbach[#]

Department of Earth, Atmospheric and Planetary Sciences, Massachusetts Institute of Technology, Cambridge, Massachusetts

Helen L. Johnson

Department of Earth Sciences, University of Oxford, Oxford, United Kingdom

David P. Marshall

Department of Physics, University of Oxford, Oxford, United Kingdom

ABSTRACT

Attributing observed variability of the Atlantic meridional overturning circulation (AMOC) to past changes in surface forcing is challenging but essential for detecting any influence of anthropogenic forcing and reducing uncertainty in future climate predictions. Here, quantitative estimates of separate contributions from wind and buoyancy forcing to AMOC variations at 25°N are obtained. These estimates are achieved by projecting observed atmospheric anomalies onto model-based dynamical patterns of AMOC sensitivity to surface wind, thermal, and freshwater forcing over the preceding 15 years. Local wind forcing is shown to dominate AMOC variability on short time scales, whereas subpolar heat fluxes dominate on decadal time scales. The reconstructed transport time series successfully reproduces most of the interannual variability observed by RAPID–MOCHA. However, the apparent decadal trend in the RAPID–MOCHA time series is not captured, requiring improved model representation of ocean adjustment to subpolar heat fluxes over at least the past two decades and highlighting the importance of sustained monitoring of the high-latitude North Atlantic.

Corresponding author address: Helen R. Pillar, Niels Bohr Institute, University of Copenhagen, Juliane Maries Vej 30, 2100 Copenhagen, Denmark.
E-mail: hpillar@nbi.ku.dk

1. Introduction

The Atlantic meridional overturning circulation (AMOC) carries a substantial amount of heat poleward in the North Atlantic and is believed to play a key role in multidecadal variations in North Atlantic sea surface temperatures (Klöwer et al. 2014) and provide a potential source of regional climate predictability (Msadek et al. 2010). The AMOC is projected to weaken over the next century in response to greenhouse gas emissions, with implications for the North Atlantic storm track

(Woollings et al. 2012), hurricane frequency (Zhang and Delworth 2006), European climate (Stouffer et al. 2006), regional sea level (Pardaens et al. 2011), and global terrestrial (Higgins and Vellinga 2004) and marine (Schmittner 2005) ecosystems. These projections are plagued by significant uncertainty, as state-of-the-art climate models diverge on both the predicted timing and amplitude of future weakening (Meehl et al. 2007) and the mean strength and variability of the present-day AMOC. Valuable observational constraints are provided by RAPID–MOCHA at 26°N, where the strength of the AMOC has been continuously monitored since 2004, exhibiting large variability on all time scales (Smeed et al. 2014), with peak-to-peak variability in excess of the mean value of 17.2 Sv (1 Sv $\equiv 10^6$ m^3 s^{-1}; McCarthy et al. 2015). Exploring the cause of these observed variations and quantifying the relative importance of various external (atmospheric) forcings versus internal (eddy induced) processes is complex (Wunsch and Heimbach 2013) but essential for understanding the sensitivity of the AMOC to future change.

The purpose of this study is to attribute recently observed AMOC variability at RAPID–MOCHA to past surface wind, thermal, and freshwater forcing. The traditional forward modeling approach to attribution involves running ensembles of perturbed experiments, changing different aspects of the surface forcing in each case and examining the impact on the modeled state. However, in a state-of-the-art ocean model, the number of possible perturbations is vast, requiring a very large ensemble to perform a comprehensive sensitivity study. Beyond the technical difficulties of implementing a large ensemble investigation, attempts to identify causal mechanisms are often restricted to statistical indicators of mutual variation between the AMOC and atmospheric forcing, lacking clear dynamical insight.

If we focus our attention on a specific metric of the evolved climate state—the AMOC at RAPID–MOCHA—it is helpful to also focus our computational resources on quantifying all potential causes of variability in this single metric (or "objective function"), as opposed to the impact of one imposed perturbation on the evolution of the entire climate state. For this, the adjoint method is a powerful tool [for accessible formal descriptions, see Errico (1997), Marotzke et al. (1999), and Heimbach (2008)], providing the local linear sensitivity of the AMOC to changes in surface forcing along the entire model trajectory. Examining how these sensitivity maps (equivalently Lagrange multipliers; Heimbach and Bugnion 2009) evolve through time reveals all viable dynamical mechanisms by which small-amplitude surface forcing perturbations may impact the AMOC at the latitude of the monitoring array.

The adjoint approach has been employed by Köhl (2005), Czeschel et al. (2010), and Heimbach et al. (2011) to explore

the sensitivity of the total northward AMOC transport across 27°N to buoyancy forcing. Czeschel et al. (2010) suggest that the AMOC may possess oscillatory sensitivity to high-latitude heat fluxes on decadal time scales. Since sensitivities must be collocated in time and space with forcing anomalies to excite variability in the modeled transport, the implications of this long-term memory for the generation of AMOC variability has yet to be fully determined.

Recently Czeschel et al. (2012) have successfully applied the adjoint approach to elucidate the driving mechanisms of the seasonal cycle in the Florida Current transport. By multiplying the associated linear sensitivities by corresponding wind stress anomalies from reanalysis, the authors are able to both reconstruct the current transport offline and provide a rigorous, physical explanation for the spatial and temporal origins of the forcing driving seasonal variability through the straits.

In this paper, we follow a similar, fundamentally mechanistic approach to attribute variations of the AMOC to the past history of surface wind, buoyancy, and freshwater forcing. The model configuration and adjoint sensitivity calculation are described in section 2. Insights into the pathways and time scales of AMOC sensitivity to air–sea flux perturbations are discussed in section 3. Separate time series of buoyancy-driven and wind-driven AMOC transport are constructed by convolving the linear sensitivities with forcing anomalies from atmospheric reanalysis and compared to recent observations from RAPID–MOCHA in section 4. A concluding discussion is given in section 5.

2. Experiment design

a. Model description

Our experiments are performed using a global configuration of the Massachussetts Institute of Technology General Circulation Model (MITgcm; Marshall et al. 1997a,b) truncated at 74°N and 78°S. The horizontal resolution is 1°, and in the vertical there are 33 levels of varying thickness increasing from 10 m at the surface to 250 m at depth. The model is driven by a repeating cycle of climatological monthly mean surface fluxes of heat, freshwater, and momentum derived from the NCEP–NCAR reanalysis product (Kalnay et al. 1996). The initial stratification is based on hydrographic observations. To prevent significant drift of the sea surface temperature and salinity, we relax the simulated surface values to climatology with a damping time scale of 2 and 6 months, respectively. Restoration of the full-depth temperature and salinity fields toward climatology is also imposed at the open portion of the northern margin. Unresolved processes associated with mixing and advection by eddies are parameterized following Redi (1982) and Gent and McWilliams (1990), respectively. The K-profile parameterization (KPP) scheme

proposed by Large et al. (1994) is also employed to represent unresolved processes entailed in vertical mixing.

Following integration over 1300 model years, no significant trends are discernible in the tracer and momentum fields. In this statistical steady state, the modeled AMOC at 25°N has an annual mean of approximately 21 Sv and a seasonal cycle with a peak-to-peak amplitude of approximately 4 Sv. Seasonal AMOC variations north of approximately 20°N are principally described by a standing pattern of amplification. A decadal mode of AMOC variability is also visible in extended time series of transport variability at latitudes north of the equator. This is weak relative to the seasonal cycle and is a common feature of both ocean-only and coupled climate models, although the key driving mechanisms are disputed (Frankcombe et al. 2010). Since the external forcing varies only on seasonal time scales, this decadal mode is an internal mode of ocean variability in our model.

b. Linear sensitivity calculation

The adjoint model computes the sensitivity of a single model metric (the objective function) to all model inputs (the "controls"). We define the objective function as the monthly mean maximum meridional overturning circulation at 25°N $\overline{\psi}_{25°N}^{month}$; the controls are surface wind stresses and fluxes of freshwater and heat. Since continental runoff is poorly represented at our model resolution, surface freshwater fluxes are defined to exclude this contribution. Since there is a notable seasonal cycle in the equilibrated state, an ensemble of 12 adjoint calculations is required (with the objective function defined as the January through December mean AMOC at 25°N) to probe the origins of monthly AMOC transport variability.

The equilibrated model is integrated for a further 20 years, during which the linear sensitivities are computed at every grid point and time step via algorithmic differentiation using the commercial tool transformation of algorithms in Fortran (TAF; Giering 2010). To obtain useful gradient information, we follow the standard practice of neglecting the highly nonlinear and discontinuous KPP scheme when forming the adjoint model (e.g., Hoteit et al. 2005) and also neglect the eddy advection scheme (Gent and McWilliams 1990) for technical reasons.

To determine whether the linear sensitivities provide a meaningful description of perturbation growth in the nonlinear GCM, we compare the AMOC at 25°N in an ensemble of forward integrations with perturbed surface forcing to that diagnosed offline using the linear sensitivities (see Pillar 2013). Consistent with earlier experiments at a similar resolution (Czeschel et al. 2010; Heimbach et al. 2011), linear sensitivities are found to be representative up to lead times of approximately 15 yr (also similar to the maximum-growth time scales of surface-forced AMOC

variability arising from nonnormal mode interaction; Zanna et al. 2012).

3. AMOC sensitivity pathways

The pathways of AMOC sensitivity to surface forcing have been previously discussed by Marotzke et al. (1999), Bugnion et al. (2006a,b), Czeschel et al. (2010), and Heimbach et al. (2011). Here we review the pertinent pathways to provide the context for the construction of the transport time series in section 4. To simplify the present discussion, we present sensitivity distributions only for the January mean AMOC $\overline{\psi}_{25°N}^{Jan}$ in Fig. 1. It is natural to discuss the evolution of the sensitivity distributions with increasing lead time from the point at which the objective function is analyzed (Bugnion et al. 2006b). As a result, propagation pathways observed in the forward model are traversed in the opposite direction in the adjoint framework.

At all lead times considered, the standard deviation of the sensitivity ensemble is at least an order of magnitude smaller than the sensitivity of the monthly mean AMOC in any given month. For visual inspection, sensitivity distributions for the January mean AMOC (Fig. 1) may therefore be considered representative of the remaining 11 members of the sensitivity ensemble. It is important to note, however, that the small variations in sensitivity across the ensemble have a notable impact on the transport calculation in section 4. This is fully addressed in a parallel study (H. Pillar et al. 2016, unpublished manuscript) where the physics controlling the seasonality of the sensitivity is explored in more detail.

a. Sensitivity to surface momentum fluxes

At a lead time of 1 month, significant sensitivity to wind stress (Figs. 1a,d) is confined to the North Atlantic basin. The sensitivity to zonal wind stress at this lead time is dominated by a broad, zonally uniform band of negative sensitivity extending across the basin width at 25°N (Fig. 1a) with a maximum amplitude of approximately $-0.4 \times 10^{-10}\,\text{Sv}\,\text{N}^{-1}$. An increase in the westerly wind stress of $0.01\,\text{N}\,\text{m}^{-2}$ across 3° of latitude ($\sim 3 \times 10^5\,\text{m}$) and along the full width of the section ($\sim 7 \times 10^6\,\text{m}$) would lead to a decrease of the AMOC at 25°N by approximately 0.84 Sv in the same month by perturbing the Ekman transport across the basin. Note that here the meridional length scale is chosen to approximate migration within the Ekman layer during the averaging period of the objective function (1 month).

At a lead time of 3 months a signature of this fast Ekman response is still visible, although the sensitivity across 25°N is now positive and flanked by bands of alternating sign (Fig. 1b). Forward sensitivity experiments (see Pillar 2013) reveal that the physics responsible for
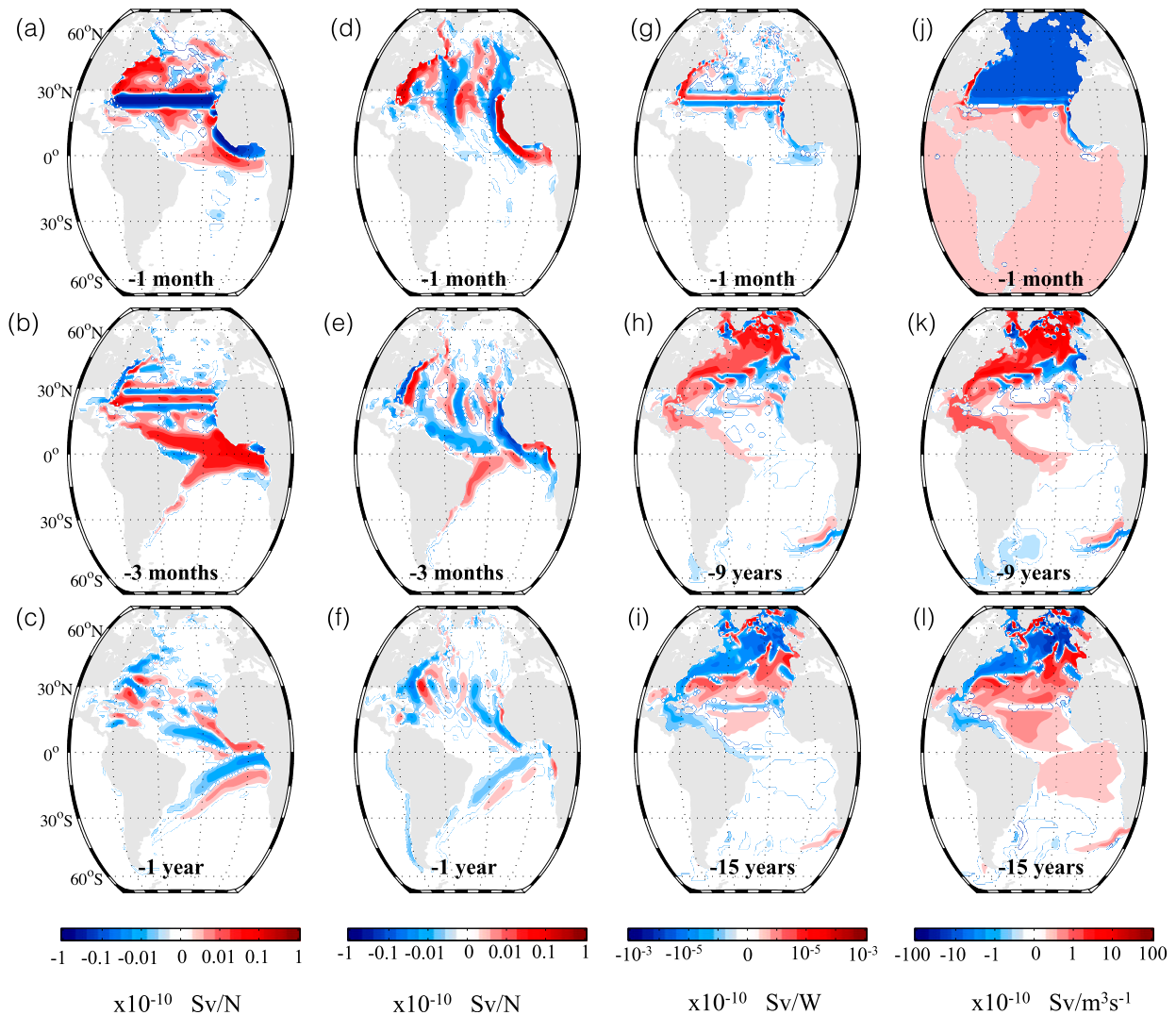
FIG. 1. Linear sensitivity of the AMOC at 25°N in January to (a)–(c) zonal wind stress, (d)–(f) meridional wind stress, (g)–(i) surface heat fluxes, and (j)–(l) surface freshwater fluxes per unit area for forcing at the indicated lead time. Surface freshwater fluxes are defined to exclude the contribution from continental runoff and ice melt and/ or calving. Positive sensitivity indicates that increased eastward wind in (a)–(c), northward wind in (d)–(f), upward heat flux in (g)–(i), or evaporation in (j)–(l) leads to an increased AMOC at 25°N. Taking (h) as an example, a unit increase in upward heat flux at a given location will change the AMOC at 25°N 9 years later by the amount shown in the color bar. The contour intervals are logarithmic to illustrate the rapid loss of sensitivity to wind forcing with increased lead time. These pathways reveal all viable dynamical mechanisms by which small-amplitude surface forcing perturbations at the lead time indicated may impact the AMOC at 25°N. Since the seasonality in the sensitivity is small, these sensitivity distributions can be considered representative of the remaining 11 months in the adjoint ensemble.

this distribution is related to the steering of pressure perturbations around the Mid-Atlantic Ridge by barotropic Rossby waves. The distribution is modified by the subsequent excitation of slower, baroclinic Rossby waves propagating westward from the western flank of the ridge (Barnier 1988). These mechanisms are also responsible for the dipole straddling the Mid-Atlantic Ridge in the sensitivity to meridional wind stress (Figs. 1d,e; see Pillar 2013). At short lead times, notable sensitivities

also occupy the upstream coastal waveguides, highlighting the importance of trapped boundary waves in the rapid adjustment of the AMOC (Johnson and Marshall 2002b; Marshall and Johnson 2013). The sign of the sensitivity in the coastal waveguides can be understood by considering the orientation of the coastline (i.e., onshore or offshore Ekman transport) and the contribution of the established pressure anomalies to the cross-basin pressure gradient and geostrophic response at 25°N.

With increased forcing lead time, AMOC sensitivity emerges to increasingly remote winds. The distributions in Figs. 1c,f reveal all locations where wind anomalies can impact the overturning at 25°N after one year and are explained as follows. Wind forcing in the tropical Atlantic interior generates pressure anomalies locally. These anomalies are first communicated to the western boundary by Rossby waves (clearly seen in Figs. 1c,f tilting eastward toward the equator because of the β effect) and subsequently to the eastern boundary at 25°N via coastal and equatorial waveguides, to impact the geostrophic overturning after 1 year. The tropics emerge as a key pathway for Rossby wave propagation in Figs. 1c,f as a result of amplification along the baroclinically unstable flanks of the subtropical gyres (Heimbach et al. 2011; Galanti and Tziperman 2003; Köhl 2005). Long Rossby waves are damped in transit by viscous dissipation at higher latitudes where propagation speeds are slower. At a lead time of 1 yr, the amplitude of AMOC sensitivity to wind stress has diminished significantly and does not reamplify (Figs. 1c,f).

b. Sensitivity to surface buoyancy fluxes

Maps of sensitivity to surface thermal and freshwater forcings reveal the same rapid teleconnections discussed above, acting on short time scales (Figs. 1g,j). A notable difference is the global extent of AMOC sensitivity to freshwater forcing at a lead time of 1 month (Fig. 1j, showing only the Atlantic basin) due to the rapid redistribution of volume around the globe by barotropic waves (Lorbacher et al. 2012). In the model, the continuity equation is formulated to allow changes in ocean volume in response to surface freshwater fluxes. Volume changes associated with surface thermal fluxes are negligible in comparison (Greatbatch 1994) and are neglected in the model. As a result the fast global barotropic adjustment is absent from the thermal forcing sensitivities (Fig. 1g).

In marked contrast to the wind forcing sensitivities, the sensitivities to surface thermal and freshwater forcings do not decrease monotonically with lead time. Instead, decadal time scales are generated by advective processes linking 25°N to high northern latitudes. Furthermore, the sign of sensitivity oscillates with forcing lead time in the North Atlantic (Czeschel et al. 2010); densification of the Gulf Stream and subpolar gyre at a lead time of 9 yr (Figs. 1h,k) strengthens the AMOC across 25°N but has an opposite effect at a lead time of 15 yr (Figs. 1i,l). This is consistent with the existence of a decadal mode of AMOC variability in the forward model integration and is due to a self-sustaining thermal Rossby mode (Huck et al. 1999; te Raa and Dijkstra 2002), modified by Gulf Stream advection and the passage of baroclinic Rossby waves radiated from the northeast Atlantic. The reader is referred to Czeschel et al. (2010) for further discussion

and evidence that this thermal Rossby mode is operating based on the sensitivity of the AMOC to temperatures on the east and west sides of the North Atlantic.

Interestingly, our results also suggest that buoyancy forcing over the Agulhas retroflection—a key source region for the warm and salty waters forming the upper limb of the AMOC—is important at lead times nearing a decade and longer. The stationarity of the sensitivity here is possibly due to prolonged recirculation at a model resolution where leakage is not well represented (Heimbach et al. 2011).

Notable sensitivity to freshwater forcing is found in the subtropical gyres of both hemispheres at lead times exceeding a decade (Fig. 1i). The suggestion is that salty anomalies, generated by increased low-latitude evaporation, are advected toward the northeast Atlantic, where they support a positive perturbation zonal density gradient and reinforce the AMOC. The subtropics do not play a significant role in the thermal Rossby mode present in the surface heat forcing sensitivities (Fig. 1i). We hypothesize that this discrepancy is due to stronger relaxation of sea surface temperature, relative to salinity, imposed in the model.

To conclude, we note that atmospheric forcing anomalies occurring outside the Atlantic basin do not appear significant for the variability of the monthly mean AMOC at 25°N on time scales less than 15 yr. Furthermore, concentration of the largest sensitivity at latitudes north of 25°N within the Atlantic basin supports the existence of an "equatorial buffer" (Johnson and Marshall 2002a,b).

4. Attribution of AMOC anomalies to surface forcing

In any given month, the response of the AMOC at 25°N to anomalies in atmospheric forcing F may be computed from the linear sensitivities as follows:

$$\Delta \overline{\psi}_{25°N}^{month} = \sum_{t=1\,month}^{memory} \iint \frac{\partial}{\partial F} \overline{\psi}_{25°N}^{month} \Delta F \, dx \, dy, \qquad (1)$$

where $\partial \overline{\psi}_{25°N}^{month}/\partial F(x, y, t)$ are the monthly mean linear sensitivities from the adjoint and $\Delta F(x, y, t)$ are the monthly anomalies about the NCEP–NCAR reanalysis climatological seasonal cycle (used to force the forward model). Integrating over the global ocean and summing over lead time t accumulates the ocean response along all adjustment pathways to provide a net AMOC anomaly $\Delta \overline{\psi}_{25°N}^{month}$. By examining how the AMOC estimate changes as the maximum forcing lead time, equivalently AMOC "memory," is increased from 1 month to 15 years, we determine the importance of long-term memory, as well as local versus remote influences, in the generation of AMOC variability at 25°N.

To obtain time series of AMOC anomaly $\Delta\overline{\psi}_{25°N}^{month}(t)$, Eq. (1) is reapplied to project different 15-yr-long periods of reanalysis forcing anomalies ΔF onto the 15-yr sensitivity history. Forcing anomalies are currently available from the NCEP–NCAR reanalysis product for January 1979–June 2015 inclusive. AMOC reconstructions accounting for the maximum (15 yr) response history accessible via the adjoint can therefore be obtained for the period January 1994–June 2015 inclusive. The reconstruction can be extended back from January 1994 to the start of the reanalysis period by continually reducing the maximum AMOC memory considered (see Fig. S1 of the supplementary material).

The surface flux anomalies are only able to generate appreciable AMOC variability at 25°N if they project strongly onto the sensitivity patterns (mapped for the January mean AMOC in Fig. 1). The reconstructed AMOC variability driven by zonal wind, meridional wind, thermal, and freshwater forcing anomalies is plotted in Fig. 2, where the contribution from each external forcing is shown separately. In each panel 180 reconstructions of the AMOC at 25°N are plotted, with the color indicating the length of time (from 1 to 180 months) over which past forcing is cumulatively accounted for [Eq. (1)].

a. Attribution to surface momentum fluxes

Wind forcing dominates AMOC variability at 25°N on short time scales (Zhao and Johns 2014; Polo et al. 2014; Biastoch et al. 2008); the zonal and meridional wind stress generate transient AMOC fluctuations of approximately ±6 and ±3 Sv, respectively, on time scales less than a year. Between consecutive months these anomalies can differ by as much as 9.5 and 2.5 Sv. Since the AMOC sensitivity to wind stress anomalies decays rapidly with time (Figs. 1a–f), interannual variability in the reconstructed AMOC time series is not significantly altered by accounting for increasingly historic wind forcing (Figs. 2a,b).

Examination of the latitudinal origins of AMOC anomalies driven by the wind reveals that, although the wind-forced AMOC variability is dominated by contributions from both the local Ekman transport (Fig. 3) and wind forcing over the upstream waveguides, remote wind stress anomalies over the subpolar gyre generate decadal variability at 25°N (Figs. 3 and 4), with an amplitude of ±1.5 and ±1.0 Sv when the response to zonal and meridional wind forcing, respectively, is accumulated over 15 years (Figs. 3f and 4f).

Wind forcing over the Northern Hemisphere subtropical gyre also drives low-frequency AMOC variability at 25°N, with a similar amplitude and phase to that generated by subpolar wind forcing (Figs. 3f and 4f). A strengthening of the AMOC at 25°N for the major part of 1995–2000 and 2006–10, as well as a weakening

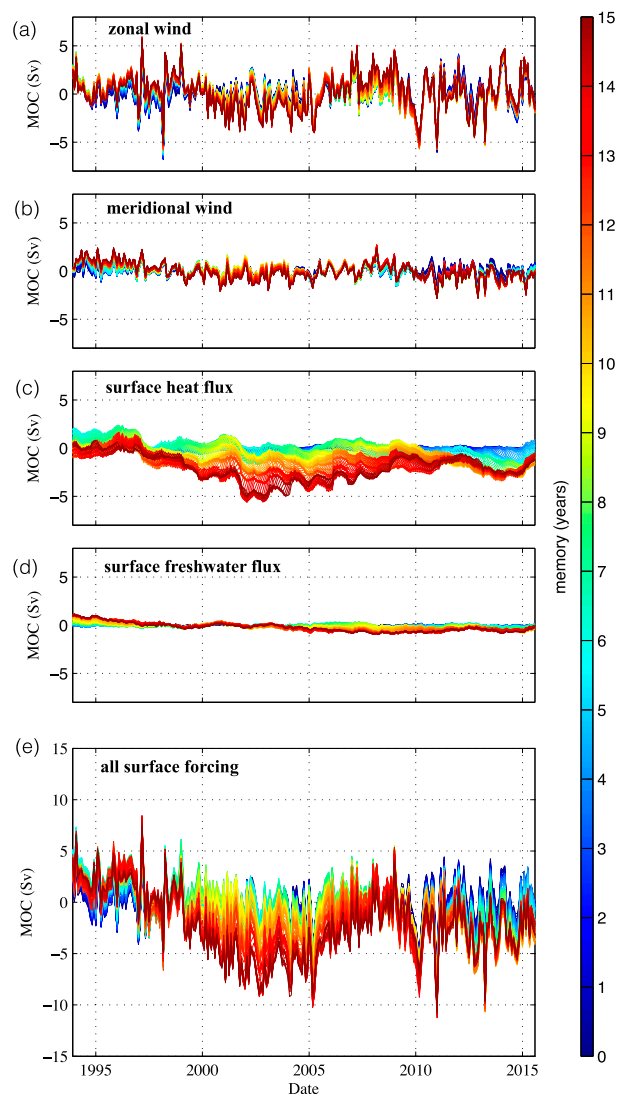
FIG. 2. AMOC variability at 25°N generated by interannual anomalies in (a) zonal wind, (b) meridional wind, (c) surface heat flux, (d) surface freshwater flux, and (e) all forcing combined [sum of transports in (a)–(d)] for the period January 1994–June 2015 inclusive. These time series are computed by convolving model-derived patterns of linear sensitivity of the AMOC to air–sea fluxes with corresponding forcing anomalies from the NCEP–NCAR reanalysis, integrating in space and accumulating in time [see Eq. (1)]. Color indicates the length of time over which past forcing is cumulatively accounted for (or, equivalently, the assumed memory of the AMOC at 25°N).

during 2000–06, is notable when zonal wind forcing at lead times exceeding approximately 5 yr is accounted for (Figs. 3d–f). The duration of this lagged response to North Atlantic Oscillation (NAO) wind forcing is in agreement with results presented by Robson et al. (2012) and Stepanov and Haines (2014).

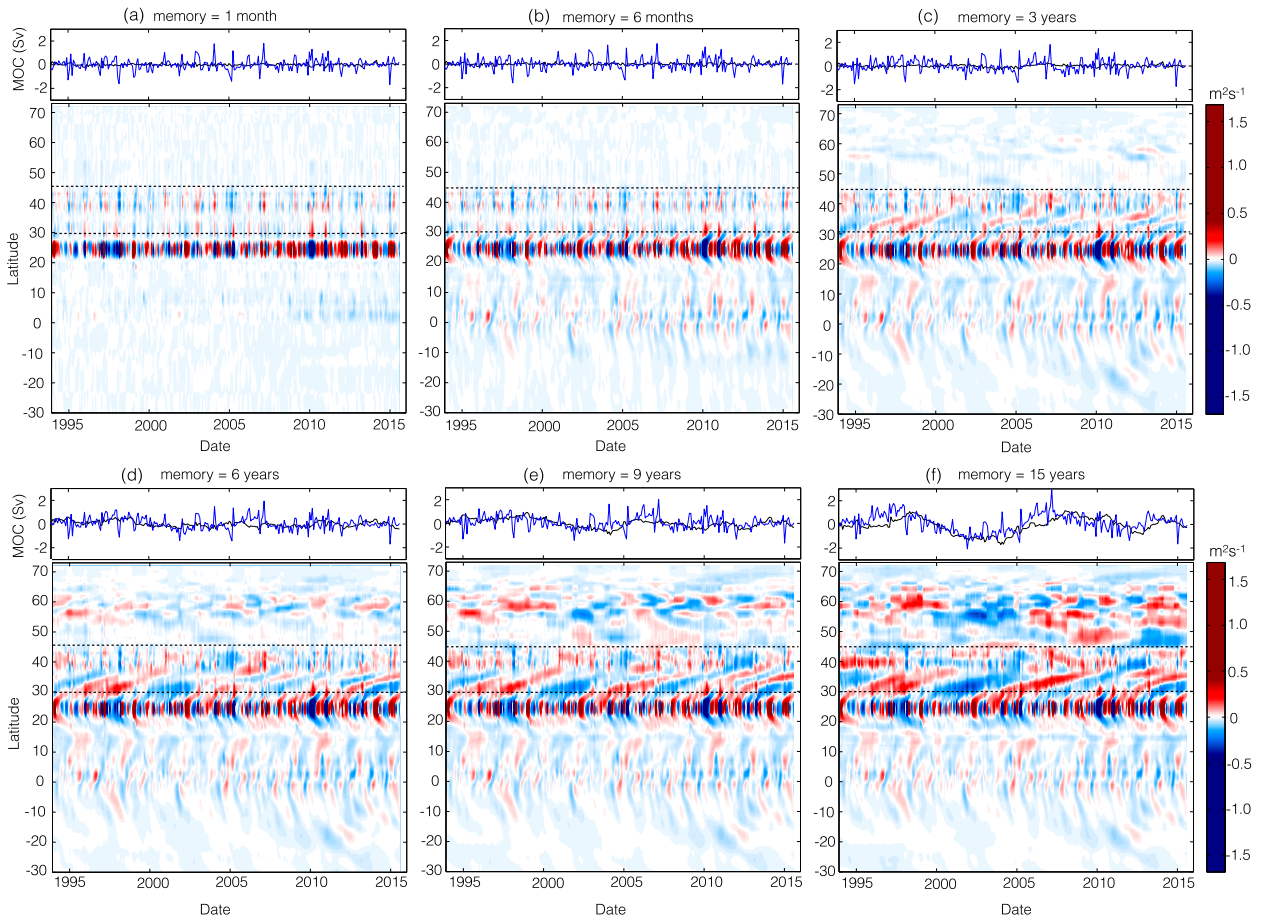The patterns shown in Figs. 3d–f are stationary in latitude–time space and amplify as AMOC memory is

FIG. 3. Hovmöller plots show the latitudinal origin of AMOC anomalies at 25°N (m² s⁻¹) driven by zonal wind forcing in the Atlantic basin [computed using Eq. (1) but without integrating meridionally]. Accompanying time series show the net contribution of the zonal wind at all Atlantic latitudes north of 45°N (black line) and at latitudes between 30° and 45°N (blue line, chosen to represent the subtropical gyre while excluding the local Ekman response) to AMOC variability at 25°N. The color bar is saturated to highlight the contribution from remote wind forcing. The assumed memory of the AMOC increases from (a) 1 month to (f) 15 years.

increased, associated with the accumulation of zonally propagating anomalies. This is consistent with the suggestion that the local Ekman pumping response to stochastic NAO-related winds at high latitudes is integrated along interior Rossby and western boundary wave characteristics to drive multidecadal variability at latitudes south of the area under direct NAO forcing (Zhai et al. 2014). High-frequency AMOC variability is restricted to generation at lower latitudes where the Rossby crossing time scale is shorter (a mechanism termed the ''Rossby buffer''; Zhai et al. 2011).

Strong hemispheric asymmetry in the patterns in Figs. 3 and 4 highlights the role played by the equatorial buffer (Johnson and Marshall 2002b, 2004), seen in the sensitivity maps (Fig. 1), in restricting the area of forcing influence. Density (or pressure) anomalies generated by surface buoyancy and momentum fluxes cannot cross the equator without strong attenuation resulting from

geostrophic constraints. High-frequency variability in the AMOC at 25°N can, however, be generated in the deep tropics (Figs. 3 and 4), where the equatorial waveguide is readily accessed and both slow interior pathways (the Rossby buffer) and geostrophic attenuation (the equatorial buffer) are avoided.

b. Attribution to surface buoyancy fluxes

Thermal forcing generates AMOC variability at 25°N of similar magnitude to that generated by wind forcing, but only on decadal time scales (Fig. 2c) and only if at least a decade of thermal forcing over the subpolar gyre is accountable (Fig. 5f) (consistent with Delworth and Mann 2000; Eden and Willebrand 2001; Yeager and Danabasoglu 2014). For example, the reconstructed thermally forced AMOC minimum in 2002/03 is associated with strong subpolar heat loss 10–15 years earlier in 1987–93, projecting onto a negative phase of thermal
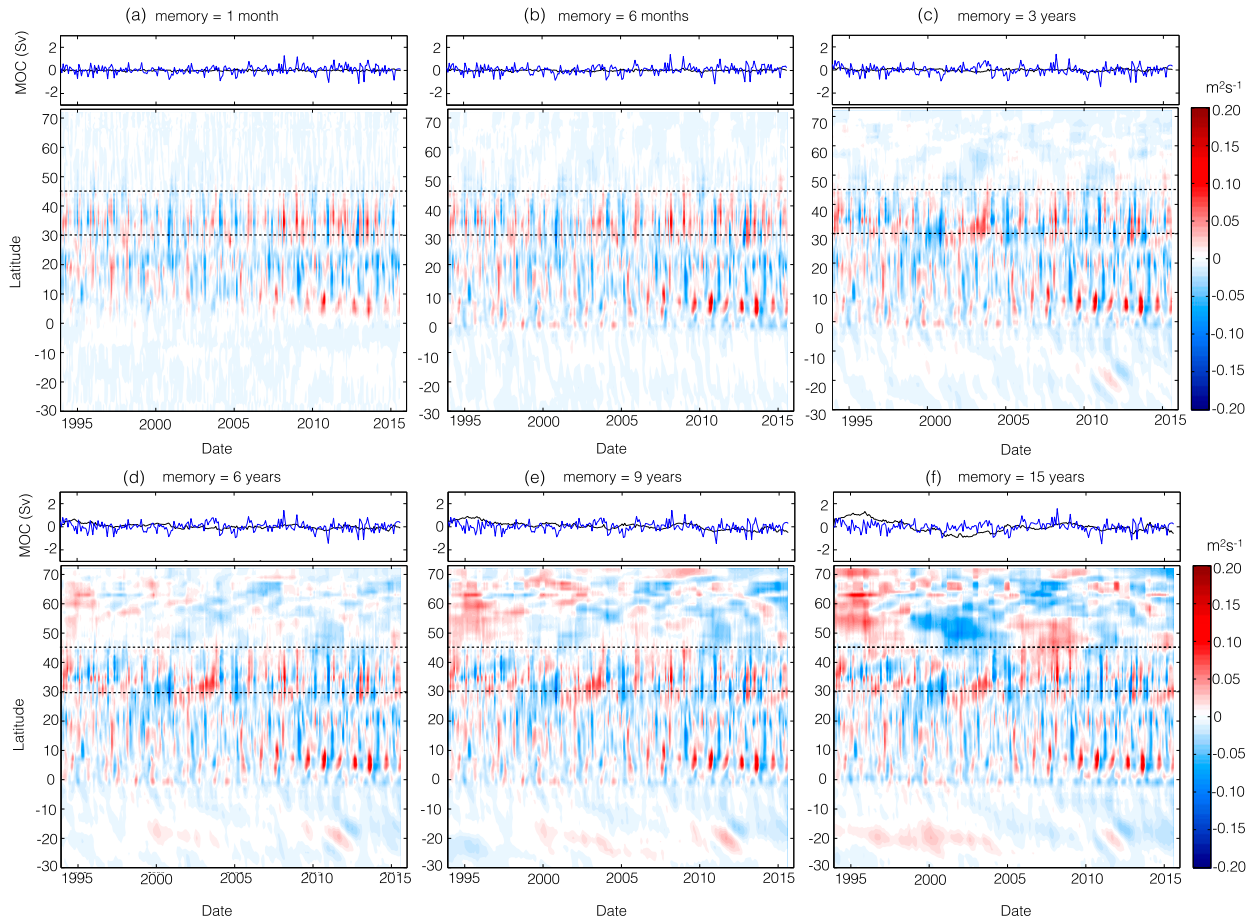
FIG. 4. As in Fig. 3, but showing the latitudinal origin of AMOC anomalies at 25°N ($m^2\,s^{-1}$) driven by meridional wind forcing in the Atlantic basin.

AMOC sensitivity (Figs. 1i and 5f). Northern Hemisphere subtropical heat fluxes also make a contribution to the low-frequency variability of the AMOC at 25°N, driving transport variations of approximately ±1 Sv when the maximum (15 yr) accumulated response is considered (Fig. 5f). Contributions from the subpolar and subtropical gyres are opposing for the periods 1993–2009 and 2010–15 for the 15-yr response history considered. Further work is required to determine how this relates to gyre-specific decadal changes in the AMOC identified in recent modeling (Bingham et al. 2007; Biastoch et al. 2008) and observational (Lozier et al. 2010) studies.

The reconstruction does not converge as thermal forcing is accumulated over an increasing time window; instead, we find that extension of the maximum lead time notably alters the thermally forced transport estimate as each additional month of historic forcing is included in the calculation [Eq. (1)]. Although the linear model does not capture the full response of the AMOC at 25°N to surface thermal forcing, it reveals both a quantifiably

acute and complex oscillatory dependence on historic heat fluxes, which would seriously hinder attribution attempts using conventional forward modeling.

Freshwater forcing is ineffective in generating significant AMOC variability at 25°N (Fig. 2d); an AMOC anomaly exceeding 1.0 Sv is only excited after the response to surface freshwater fluxes is accumulated over 11 years. This relative ineffectiveness is due to a spatial mismatch between the forcing and sensitivity maps for the period examined; the largest freshwater anomalies are located in the deep tropics where the sensitivity to freshwater fluxes is weak (Fig. 1f). Despite this low sensitivity, tropical freshwater injection makes a major contribution to the total freshwater-forced AMOC anomaly at 25°N (Fig. 6f).

The freshwater contribution from continental runoff and ice melt/calving is omitted in our calculation because of both poor representation in our coarse-resolution model (preventing calculation of meaningful sensitivity patterns) and the lack of observational
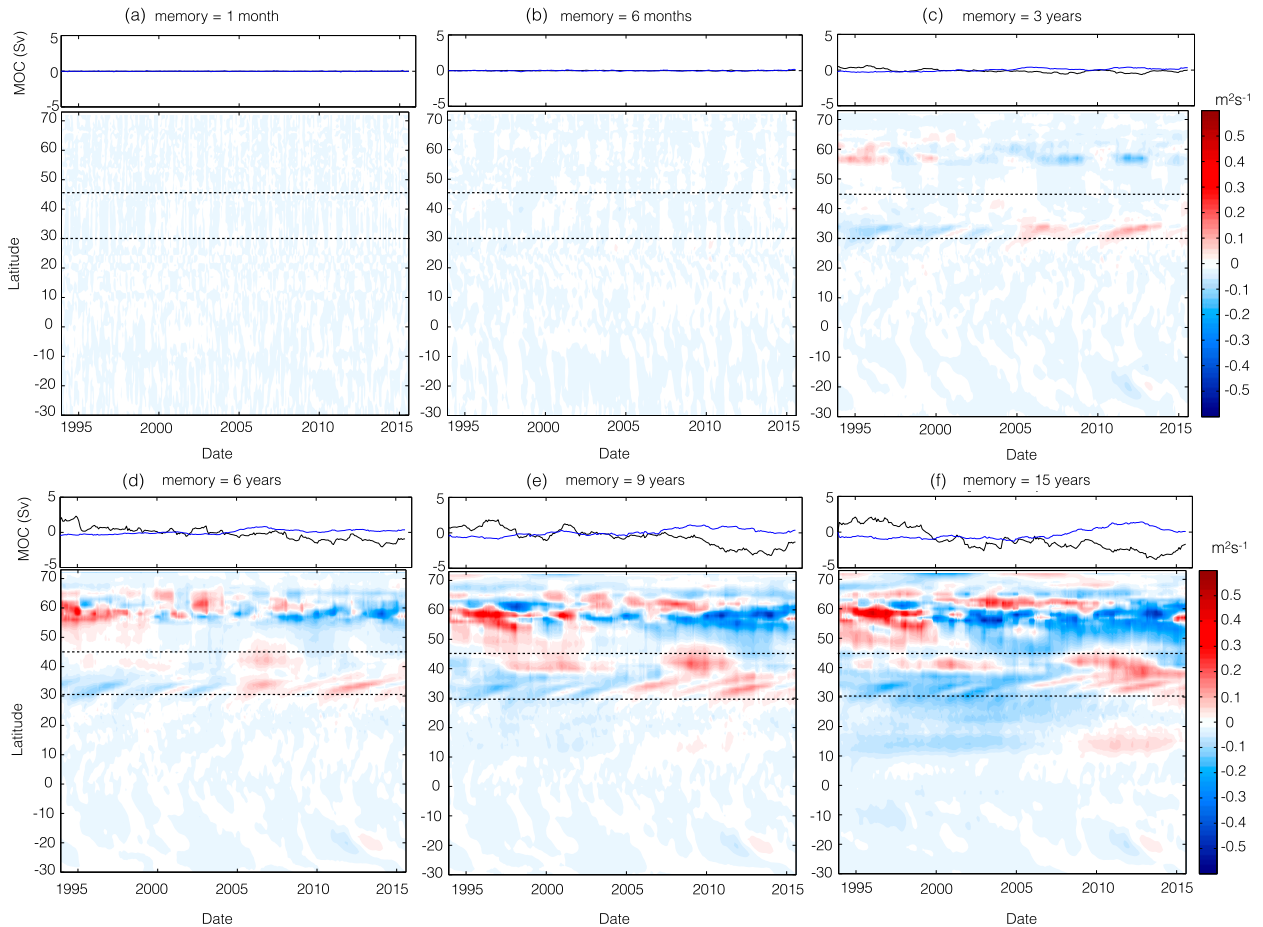
FIG. 5. As in Fig. 3, but showing the latitudinal origin of AMOC anomalies at 25°N (m^2 s^{-1}) driven by surface thermal forcing in the Atlantic basin.

constraints (preventing a useful estimate of AMOC transport driven by global runoff and ice melt and/or calving variations). It is noted that ice discharge from Greenland's outlet glaciers, together with sea ice export from the Arctic on both sides of Greenland, is likely to inject freshwater in regions of high AMOC sensitivity (Figs. 1j–l). Furthermore, ice melt/calving fluxes into the Labrador and Irminger Seas have made a substantial and increasing contribution to the total freshwater injection in the high-latitude North Atlantic in recent years (Bamber et al. 2012). Accounting for this source of freshwater forcing could produce AMOC anomalies at 25°N exceeding the 1 Sv shown in Fig. 6f [e.g., see regional simulations by Weijer et al. (2012)].

c. Comparison to observed AMOC variability

The combined response of the AMOC at 25°N to wind, thermal, and freshwater forcing is shown in Fig. 2e. The net reconstructed AMOC variability ranges between −11 and +8 Sv, with wind forcing dominating after 2007.

Thermal forcing played a large role prior to 2007, and there is consequently greater uncertainty in that period resulting from the nonconvergence of the thermally forced AMOC reconstruction. Superimposing the reconstruction from Fig. 2e onto the modeled seasonal cycle on the AMOC at 25°N (section 2a) provides an estimate of externally forced AMOC variability at 25°N for comparison with observations at the RAPID–MOCHA (Fig. 7).

The full sensitivity-based reconstruction shows remarkable agreement with the RAPID–MOCHA time series on seasonal to interannual time scales (Fig. 7). The general weakening of the reconstructed transport in 2009/10 and the amplitude of the winter minima in 2009/10 and 2010/11 are comparable to published observations (Smeed et al. 2014; Srokosz et al. 2012) and due to both the instantaneous Ekman response to local wind stress anomalies (Fig. 8a) and the nonlocal response to remote wind stress anomalies (Fig. 8b). This finding is consistent with Roberts et al. (2013) but based on dynamical rather than statistical attribution,
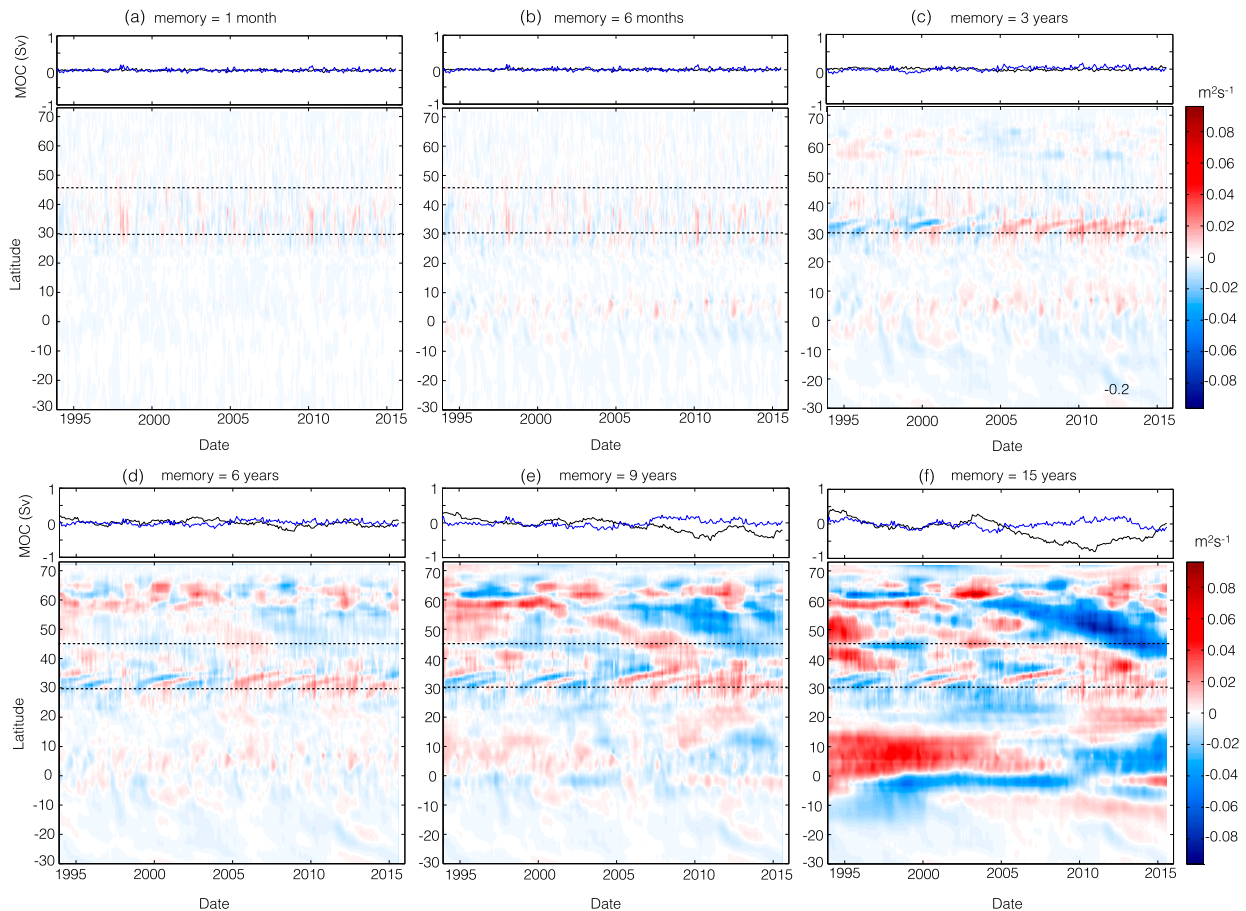
FIG. 6. As in Fig. 3, but showing the latitudinal origin of AMOC anomalies at 25°N (m² s⁻¹) driven by surface freshwater forcing in the Atlantic basin.

demonstrating that despite the limitations of our ocean circulation model and the assumption of linearity, adjoint sensitivities can provide a meaningful quantitative description of perturbation growth over the time window considered.

Our reconstructed transport time series does not correctly capture observed variability at RAPID–MOCHA during the first few years of continuous monitoring (Fig. 7). Notably, the AMOC is observed to be strongest during 2004–06 when our thermally forced transport
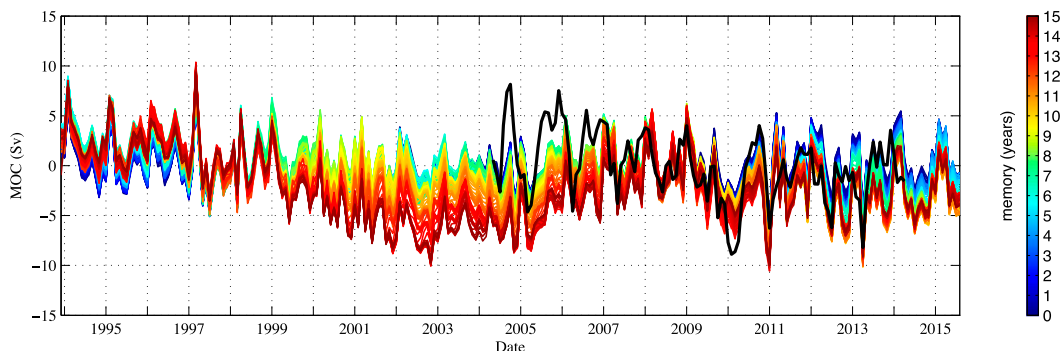

FIG. 7. Reconstructed transport as in Fig. 2e, but superimposed on the modeled seasonal cycle of the AMOC at 25°N to recover the full AMOC at 25°N for comparison with observations at the RAPID–MOCHA (black line). Note that the transport anomalies given in Eq. (1)—and shown in Fig. 2—are computed as departures from the modeled seasonal cycle of the AMOC at 25°N.
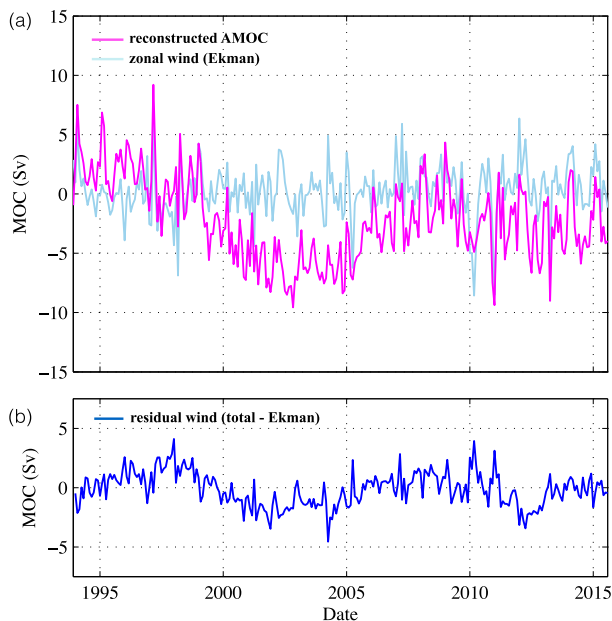
FIG. 8. (a) Reconstructed transport (pink line) as in Fig. 7, but only the reconstruction accumulating the full (15 yr) response history accessible via the adjoint is retained. The majority of the interannual variability in the full reconstruction is explained by the instantaneous Ekman response (light blue line), computed as the cross-basin integral of $-\Delta\tau^x/\rho_0 f$, where ρ_0 is a reference density, f is the Coriolis parameter, and $\Delta\tau^x$ are zonal wind anomalies (about the NCEP–NCAR reanalysis climatology) in the same month. (b) The residual wind contribution is computed as the difference between the zonal wind contribution to the AMOC in Fig. 2a and the Ekman transport. Although the contemporaneous zonal wind is largely responsible for the strong winter minima in 2009/10 and 2010/11, AMOC anomalies as large as ~5 Sv result from remote generation of density anomalies, which subsequently propagate to 25°N via the coastal pathways indicated in Figs. 1a–c. This highlights the importance of accounting for the impact of both local and remote surface forcings [contained within the reconstruction in (a); pink line] in understanding observed variability at the RAPID–MOCHA.

estimate (Fig. 2c) contributes to an overall negative AMOC anomaly at 25°N in our reconstruction. Errors in our thermally forced AMOC estimate could arise from both our inability to account for the contribution from heat fluxes at lead times exceeding 15 yr and the misrepresentation of low-frequency variability in the forward model.

5. Summary and discussion

We have explored the atmospheric origins of subannual and lower-frequency variability of the AMOC at 25°N in a noneddying ocean model using a numerical adjoint. We are able to explore the impact of forcing anomalies at lead times up to 15 yr and cleanly separate estimated transports from surface fluxes of zonal and meridional momentum, heat, and freshwater. Sensitivity

distributions highlight the role of Rossby waves, coastally trapped waves, and advective pathways in carrying disturbances generated across the global ocean surface to 25°N in the Atlantic. Consistent with previous studies, the modeled AMOC at this latitude possesses only short memory (of less than a year) to typical wind stress anomalies. In contrast, significant memory to buoyancy forcing persists on multidecadal time scales because of the excitation of a thermal-Rossby-type mode by large-scale low-frequency changes in the buoyancy forcing.

The short memory of the AMOC at 25°N to wind anomalies and the potency of local instantaneous wind forcing allows for easy attribution when the wind forcing is strong (e.g., in the case of the "double dip" observed at 26°N). Since much of the variability in the observed RAPID–MOCHA time series to date appears to have been wind driven, we suggest that ocean eddies cannot have been responsible for a substantial fraction of observed interannual variability in the AMOC, as has been recently argued (Thomas and Zhai 2013). This is encouraging for the prospect of gaining a dynamics-based and quantitative understanding of past variability in the AMOC on interannual time scales from longer atmospheric reanalysis datasets. It also encourages extending our investigation to compare the sensitivity of the AMOC at 25°N with AMOC sensitivity at other latitudes, such as 16°N where the Meridional Overturning Variability Experiment (MOVE) array spans the western part of the basin.

The long memory (exceeding 15 yr) of the AMOC at 25°N to surface buoyancy forcing makes attribution a serious challenge during periods when the wind forcing does not dominate AMOC variations. On decadal time scales, we show that the observed and reconstructed AMOC time series diverge as a result of the dominance of historic subpolar thermal forcing anomalies combined with uncertainties in the reanalysis product and deficiencies in the ocean model. Notably, the details of the low-frequency variability present in the forward integration are dependent upon the model configuration, in particular the model resolution, mixing coefficients, surface boundary conditions, and restoring at the northern margin. These factors affect the simulated response to high-latitude buoyancy forcing (e.g., MacMartin et al. 2013) and consequently the amplitude and time scales of sensitivity (Czeschel et al. 2010; Heimbach et al. 2011). Stochastic eddy-induced variability—neglected in our model—may also play a secondary role (Thomas and Zhai 2013).

Our results suggest that a full understanding of observed AMOC variations requires knowledge of a long atmospheric forcing and oceanic response history. Because of the lack of observations, the latter is only accessible using

(imperfect) numerical models. Although we are unable to access earlier periods of the response history using our linear sensitivity analysis, there is support for the suggestion that existing long time series of large-scale high-latitude surface buoyancy-related metrics (e.g., the North Atlantic Oscillation) could serve as useful predictors of low-frequency AMOC variations at 25°N (Ortega et al. 2011; Pohlmann et al. 2013). Our results underline the importance of new initiatives such as the Overturning in the Subpolar North Atlantic Program (OSNAP) focused on observing and physically interpreting the role of the subpolar North Atlantic in driving the AMOC and providing potential climate predictability on decadal time scales.

REFERENCES

Bamber, J., M. van den Broeke, J. Ettema, J. Lenaerts, and E. Rignot, 2012: Recent large increases in freshwater fluxes from Greenland into the North Atlantic. *Geophys. Res. Lett.*, **39**, L19501, doi:10.1029/2012GL052552.

Barnier, B., 1988: A numerical study on the influence of the Mid-Atlantic Ridge on nonlinear first-mode baroclinic Rossby waves generated by seasonal winds. *J. Phys. Oceanogr.*, **18**, 417–433, doi:10.1175/1520-0485(1988)018<0417:ANSOTI>2.0.CO;2.

Biastoch, A., C. W. Böning, J. Getzlaff, J.-M. Molines, and G. Madec, 2008: Causes of interannual–decadal variability in the meridional overturning circulation of the North Atlantic Ocean. *J. Climate*, **21**, 6599–6615, doi:10.1175/2008JCLI2404.1.

Bingham, R. J., C. W. Hughes, V. Roussenov, and R. G. Williams, 2007: Meridional coherence of the North Atlantic meridional overturning circulation. *Geophys. Res. Lett.*, **34**, L23606, doi:10.1029/2007GL031731.

Bugnion, V., C. Hill, and P. Stone, 2006a: An adjoint analysis of the meridional overturning circulation in an ocean model. *J. Climate*, **19**, 3732–3750, doi:10.1175/JCLI3787.1.

——, ——, and ——, 2006b: An adjoint analysis of the meridional overturning circulation in a hybrid coupled model. *J. Climate*, **19**, 3751–3767, doi:10.1175/JCLI3821.1.

Czeschel, L., D. Marshall, and H. L. Johnson, 2010: Oscillatory sensitivity of Atlantic overturning to high-latitude forcing. *Geophys. Res. Lett.*, **37**, L10601, doi:10.1029/2010GL043177.

——, C. Eden, and R. Greatbatch, 2012: On the driving mechanism of the annual cycle of the Florida Current transport. *J. Phys. Oceanogr.*, **42**, 824–839, doi:10.1175/JPO-D-11-0109.1.

Delworth, T., and M. Mann, 2000: Observed and simulated multidecadal variability in the Northern Hemisphere. *Climate Dyn.*, **16**, 661–676, doi:10.1007/s003820000075.

Eden, C., and J. Willebrand, 2001: Mechanisms of interannual to decadal variability of the North Atlantic circulation. *J. Climate*, **14**, 2266–2280, doi:10.1175/1520-0442(2001)014<2266:MOITDV>2.0.CO;2.

Errico, R., 1997: What is an adjoint model? *Bull. Amer. Meteor. Soc.*, **78**, 2577–2591, doi:10.1175/1520-0477(1997)078<2577:WIAAM>2.0.CO;2.

Frankcombe, L. M., A. von der Heydt, and H. Dijkstra, 2010: North Atlantic multidecadal climate variability: An investigation of dominant time scales and processes. *J. Climate*, **23**, 3626–3638, doi:10.1175/2010JCLI3471.1.

Galanti, E., and E. Tziperman, 2003: A midlatitude–ENSO teleconnection mechanism via baroclinically unstable long Rossby waves. *J. Phys. Oceanogr.*, **33**, 1877–1888, doi:10.1175/1520-0485(2003)033<1877:AMTMVB>2.0.CO;2.

Gent, P., and J. C. McWilliams, 1990: Isopycnal mixing in ocean circulation models. *J. Phys. Oceanogr.*, **20**, 150–155, doi:10.1175/1520-0485(1990)020<0150:IMIOCM>2.0.CO;2.

Giering, R., 2010: Transformation of algorithms in Fortran Version 1.15 (TAF Version 1.9.70). FastOpt.

Greatbatch, R. J., 1994: A note on the representation of steric sea level in models that conserve volume rather than mass. *J. Geophys. Res.*, **99**, 12 767–12 771, doi:10.1029/94JC00847.

Heimbach, P., 2008: The MITgcm/ECCO adjoint modelling infrastructure. CLIVAR Exchanges, No. 13, International CLIVAR Project Office, Southampton, United Kingdom, 13–17.

——, and V. Bugnion, 2009: Greenland ice sheet volume sensitivity to basal, surface, and initial conditions, derived from an adjoint model. *Ann. Glaciol.*, **50**, 67–80, doi:10.3189/172756409789624256.

——, C. Wunsch, R. Ponte, G. Forget, C. Hill, and J. Utke, 2011: Timescales and regions of the sensitivity of Atlantic meridional volume and heat transport: Toward observing system design. *Deep-Sea Res. II*, **58**, 1858–1879, doi:10.1016/j.dsr2.2010.10.065.

Higgins, P., and M. Vellinga, 2004: Ecosystem responses to abrupt climate change: Teleconnections, scale and the hydrological cycle. *Climatic Change*, **64**, 127–142, doi:10.1023/B:CLIM.0000024672.41571.ba.

Hoteit, I., B. Cornuelle, A. Köhl, and D. Stammer, 2005: Treating strong adjoint sensitivities in tropical eddy-permitting variational data assimilation. *Quart. J. Roy. Meteor. Soc.*, **131**, 3659–3682, doi:10.1256/qj.05.97.

Huck, T., A. Colin de Verdiere, and A. Weaver, 1999: Interdecadal variability of the thermohaline circulation in box-ocean models forced by fixed surface fluxes. *J. Phys. Oceanogr.*, **29**, 865–892, doi:10.1175/1520-0485(1999)029<0865:IVOTTC>2.0.CO;2.

Johnson, H., and D. Marshall, 2002a: Localization of abrupt change in the North Atlantic thermohaline circulation. *Geophys. Res. Lett.*, **29**, 1083, doi:10.1029/2001GL014140.

——, and ——, 2002b: A theory for surface Atlantic response to thermohaline variability. *J. Phys. Oceanogr.*, **32**, 1121–1132, doi:10.1175/1520-0485(2002)032<1121:ATFTSA>2.0.CO;2.

——, and ——, 2004: Global teleconnections of meridional overturning circulation anomalies. *J. Phys. Oceanogr.*, **34**, 1702–1722, doi:10.1175/1520-0485(2004)034<1702:GTOMOC>2.0.CO;2.

Kalnay, E., and Coauthors, 1996: The NCEP/NCAR 40-Year Reanalysis Project. *Bull. Amer. Meteor. Soc.*, **77**, 437–471, doi:10.1175/1520-0477(1996)077<0437:TNYRP>2.0.CO;2.

Klöwer, M., M. Latif, H. Ding, R. J. Greatbatch, and W. Park, 2014: Atlantic meridional overturning circulation and the prediction of North Atlantic sea surface temperature. *Earth Planet. Sci. Lett.*, **406**, 1–6, doi:10.1016/j.epsl.2014.09.001.

Köhl, A., 2005: Anomalies of meridional overturning: Mechanisms in the North Atlantic. *J. Phys. Oceanogr.*, **35**, 1455–1472, doi:10.1175/JPO2767.1.

Large, W. G., J. C. McWilliams, and S. C. Doney, 1994: Oceanic vertical mixing: A review and a model with a nonlocal boundary layer parameterization. *Rev. Geophys.*, **32**, 363–403, doi:10.1029/94RG01872.

Lorbacher, K., S. Marsland, J. Church, S. Griffies, and D. Stammer, 2012: Rapid barotropic sea level rise from ice sheet melting. *J. Geophys. Res.*, **117**, C06003, doi:10.1029/2011JC007733.

Lozier, S., V. Roussenov, M. Reed, and R. Williams, 2010: Opposing decadal changes for the North Atlantic meridional overturning circulation. *Nat. Geosci.*, **3**, 728–734, doi:10.1038/ngeo947.

MacMartin, D., E. Tziperman, and L. Zanna, 2013: Frequency domain multimodel analysis of the response of Atlantic meridional overturning circulation to surface forcing. *J. Climate*, **26**, 8323–8340, doi:10.1175/JCLI-D-12-00717.1.

Marotzke, J., R. Giering, K. Zhang, D. Stammer, C. Hill, and T. Lee, 1999: Construction of the adjoint MIT ocean general circulation model and application to Atlantic heat transport sensitivity. *J. Geophys. Res.*, **104**, 29 529–29 547, doi:10.1029/1999JC900236.

Marshall, D., and H. Johnson, 2013: Propagation of meridional circulation anomalies along western and eastern boundaries. *J. Phys. Oceanogr.*, **43**, 2699–2717, doi:10.1175/JPO-D-13-0134.1.

Marshall, J. C., A. Adcroft, C. Hill, L. Perelman, and C. Heisey, 1997a: A finite-volume, incompressible Navier Stokes model for studies of the ocean on parallel computers. *J. Geophys. Res.*, **102**, 5753–5766, doi:10.1029/96JC02775.

——, C. Hill, L. Perelman, and A. Adcroft, 1997b: Hydrostatic, quasihydrostatic, and nonhydrostatic ocean modeling. *J. Geophys. Res.*, **102**, 5733–5752, doi:10.1029/96JC02776.

McCarthy, G., and Coauthors, 2015: Measuring the Atlantic meridional overturning at 26°N. *Prog. Oceanogr.*, **130**, 91–111, doi:10.1016/j.pocean.2014.10.006.

Meehl, G., and Coauthors, 2007: Global climate projections. *Climate Change 2007: The Physical Science Basis*, S. Solomon et al., Eds., Cambridge University Press, 747–846. [Available online at https://www.ipcc.ch/pdf/assessment-report/ar4/wg1/ar4-wg1-chapter10.pdf.]

Msadek, R., K. Dixon, T. Delworth, and W. Hurlin, 2010: Assessing the predictability of the Atlantic meridional overturning circulation and associated fingerprints. *Geophys. Res. Lett.*, **37**, L19608, doi:10.1029/2010GL044517.

Ortega, P., E. Hawkins, and R. Sutton, 2011: Processes governing the predictability of the Atlantic meridional overturning circulation in a coupled GCM. *Climate Dyn.*, **37**, 1771–1782, doi:10.1007/s00382-011-1025-1.

Pardaens, A., J. Gregory, and J. Lowe, 2011: A model study of factors influencing projected changes in regional sea level over the twenty-first century. *Climate Dyn.*, **36**, 2015–2033, doi:10.1007/s00382-009-0738-x.

Pillar, H., 2013: Sensitivity of the Atlantic meridional overturning circulation to surface forcing. Ph.D. thesis, University of Oxford, 274 pp.

Pohlmann, H., D. Smith, M. Balmaseda, N. Keenlyside, S. Masina, D. Matei, W. Müller, and P. Rogel, 2013: Predictability of the mid-latitude Atlantic meridional overturning circulation in a multi-model system. *Climate Dyn.*, **41**, 775–785, doi:10.1007/s00382-013-1663-6.

Polo, I., J. Robson, R. Sutton, and M. Alonso Balmaseda, 2014: The importance of wind and buoyancy forcing for the boundary density variations and the geostrophic component of the AMOC at 26°N. *J. Phys. Oceanogr.*, **44**, 2387–2408, doi:10.1175/JPO-D-13-0264.1.

Redi, M., 1982: Oceanic isopycnal mixing by coordinate rotation. *J. Phys. Oceanogr.*, **12**, 1154–1158, doi:10.1175/1520-0485(1982)012<1154:OIMBCR>2.0.CO;2.

Roberts, C., and Coauthors, 2013: Atmosphere drives recent interannual variability of the Atlantic meridional overturning circulation at 26.5°N. *Geophys. Res. Lett.*, **40**, 5164–5170, doi:10.1002/grl.50930.

Robson, J., R. Sutton, K. Lohmann, D. Smith, and M. Palmer, 2012: Causes of the rapid warming of the North Atlantic Ocean in the mid-1990s. *J. Climate*, **25**, 4116–4134, doi:10.1175/JCLI-D-11-00443.1.

Schmittner, A., 2005: Decline of the marine ecosystem caused by a reduction in the Atlantic overturning circulation. *Nature*, **434**, 628–633, doi:10.1038/nature03476.

Smeed, D., and Coauthors, 2014: Observed decline of the Atlantic meridional overturning circulation 2004–2012. *Ocean Sci.*, **10**, 29–38, doi:10.5194/os-10-29-2014.

Srokosz, M., M. Baringer, H. Bryden, S. Cunningham, T. Delworth, S. Lozier, J. Marotzke, and R. Sutton, 2012: Past, present, and future changes in the Atlantic meridional overturning circulation. *Bull. Amer. Meteor. Soc.*, **93**, 1663–1676, doi:10.1175/BAMS-D-11-00151.1.

Stepanov, V., and K. Haines, 2014: Mechanisms of Atlantic meridional overturning circulation variability simulated by the NEMO model. *Ocean Sci.*, **10**, 645–656, doi:10.5194/os-10-645-2014.

Stouffer, R., and Coauthors, 2006: Investigating the causes of the response of the thermohaline circulation to past and future climate changes. *J. Climate*, **19**, 1365–1387, doi:10.1175/JCLI3689.1.

te Raa, L., and H. Dijkstra, 2002: Instability of the thermohaline ocean circulation on interdecadal timescales. *J. Phys. Oceanogr.*, **32**, 138–160, doi:10.1175/1520-0485(2002)032<0138:IOTTOC>2.0.CO;2.

Thomas, M. D., and X. Zhai, 2013: Eddy-induced variability of the meridional overturning circulation in a model of the North Atlantic. *Geophys. Res. Lett.*, **40**, 2742–2747, doi:10.1002/grl.50532.

Weijer, W., M. Maltrud, M. Hecht, H. Dijkstra, and M. Kliphuis, 2012: Response of the Atlantic Ocean circulation to Greenland ice sheet melting in a strongly-eddying ocean model. *Geophys. Res. Lett.*, **39**, L09606, doi:10.1029/2012GL051611.

Woollings, T., J. Gregory, J. Pinto, M. Reyers, and D. Brayshaw, 2012: Response of the North Atlantic storm track to climate change shaped by ocean–atmosphere coupling. *Nat. Geosci.*, **5**, 313–317, doi:10.1038/ngeo1438.

Wunsch, C., and P. Heimbach, 2013: Two decades of the Atlantic overturning circulation: Anatomy, variations, extremes, prediction, and overcoming its limitations. *J. Climate*, **26**, 7167–7186, doi:10.1175/JCLI-D-12-00478.1.

Yeager, S., and G. Danabasoglu, 2014: The origins of late-twentieth-century variations in the large-scale North Atlantic circulation. *J. Climate*, **27**, 3222–3247, doi:10.1175/JCLI-D-13-00125.1.

Zanna, L., P. Heimbach, A. Moore, and E. Tziperman, 2012: Upper-ocean singular vectors of the North Atlantic climate with implications for linear predictability and variability. *Quart. J. Roy. Meteor. Soc.*, **138**, 500–513, doi:10.1002/qj.937.

Zhai, X., H. L. Johnson, and D. P. Marshall, 2011: A model of Atlantic heat content and sea level change in response to

thermohaline forcing. *J. Climate*, **24**, 5619–5632, doi:10.1175/JCLI-D-10-05007.1.

——, ——, and ——, 2014: A simple model of the response of the Atlantic to the North Atlantic Oscillation. *J. Climate*, **27**, 4052–4069, doi:10.1175/JCLI-D-13-00330.1.

Zhang, R., and T. Delworth, 2006: Impact of Atlantic multi-decadal oscillations on India/Sahel rainfall and Atlantic hurricanes. *Geophys. Res. Lett.*, **33**, L17712, doi:10.1029/2006GL026267.

Zhao, J., and W. Johns, 2014: Wind-forced interannual variability of the Atlantic meridional overturning circulation at 26.5°N. *J. Geophys. Res. Oceans*, **119**, 2403–2419, doi:10.1002/2013JC009407.